Identification of Protein Side Chains near the Membrane−Aqueous Interface: A Site-Directed Spin Labeling Study of KcsA†

Adrian Gross*,‡ and Wayne L. Hubbell*

Jules Stein Eye Institute and Department of Chemistry and Biochemistry, University of California, Los Angeles, California 90095

Received October 3, 2001; Revised Manuscript Received November 8, 2001

ABSTRACT: This study presents an approach to identifying surface residues on membrane proteins that are exposed toward the membrane−aqueous interface. The method employs a lipid Ni(II) chelate that localizes the metal ion to a region near the membrane−aqueous interface. Lateral diffusion of the lipid chelate results in Heisenberg exchange (HE) with nitroxide side chains in the protein only if direct contact occurs between the paramagnetic species during a collision. Thus, HE serves as a signature for residues facing the bilayer in the neighborhood of the membrane−aqueous interface. To evaluate the method, 13 surface residues on the extracellular half of KcsA, a prokaryotic potassium channel of known structure, were examined for HE with the Ni(II) chelate. The HE rate between the two species is found to depend strongly on the vertical position of the nitroxide with respect to the membrane−aqueous interface. Nitroxides introduced near the interface experience relatively high HE rates, whereas nitroxides that are immersed in the bilayer interior or sterically sheltered from collision experience low or undetectable rates. The results indicate that residues near the interface can be identified on the basis of their high rates of collision with the headgroup region of the bilayer.

In recent years, membrane proteins have increasingly become targets of structural studies. But despite important progress, structure determination of membrane proteins by crystallographic means remains a relatively rare occurrence in light of the fact that membrane proteins make up an estimated 30% of all proteins (*1*), but less than 0.3% of all known structures. In the absence of a general approach to obtaining high-quality crystals of membrane proteins, structure prediction algorithms can employ the primary sequence of membrane proteins in a search for clues about how the protein may fold. For example, the low-dielectric environment of the phospholipid bilayer interior imposes severe restrictions on the folding of membrane proteins and requires that the protein match the chemical properties of its exposed surface to that of the local environment. Consequently, long stretches of predominantly hydrophobic residues are required to span the hydrophobic part of the lipid bilayer. Moreover, a position-dependent preference for certain amino acids is evident at the water−lipid interface, where aromatic residues (Trp and Tyr) are particularly abundant (*2*, *3*). Under these circumstances, identification of residues exposed toward the membrane−aqueous interface can be expected to significantly reduce the number of possible folds that a membrane protein can adopt. In this paper, we present an experimental approach to identifying such residues.

The method is based on site-directed spin labeling, a structural technique that involves the introduction of a paramagnetic nitroxide side chain in a protein at a substituted cysteine residue. The general approach of this technique has been discussed in a number of recent reviews (*4*−*8*). The commonly employed nitroxide side chain, designated R1,[1] is generated by reaction of cysteine with the methanethiosulfonate reagent (**I**), as shown in Figure 1. The EPR of the attached nitroxide provides information about the local structural environment of R1 in the protein, as well as topographical features of the protein relative to the membrane. The EPR spectrum of R1 can be perturbed by the proximity of a second paramagnetic species. The mechanism of perturbation can be static or dynamic magnetic dipolar interactions, or Heisenberg exchange (HE). The magnetic dipolar interactions are through-space and distance-dependent, and have been used to estimate the interspin distance between nitroxide pairs or between a nitroxide radical and a protein-bound paramagnetic metal ion (*9*−*11*). The HE interaction requires orbital overlap between the paramagnetic species that are involved, and thus requires contact during

† This work was supported by NIH Grant GM58568 (A.G.), NIH Grant EY05216 (W.L.H.), and the Jules Stein Professorship Endowment (W.L.H.).

* To whom correspondence should be addressed. A.G.: phone, (312) 503-3375; fax, (312) 503-5349; e-mail, a-gross@northwestern.edu. W.L.H.: phone, (310) 206-8831; fax, (310) 794-2144; e-mail, hubbellw@jsei.ucla.edu.

‡ Current address: Department of Molecular Pharmacology and Biological Chemistry, Northwestern University Medical School, Chicago, IL 60611.

[1] Abbreviations: CHAPS, 3-[(3-cholamidopropyl)dimethylammonio]-1-propanesulfonate; EDTA, ethylenediaminetetraacetic acid; EPR, electron paramagnetic resonance; HE, Heisenberg exchange; NiEDDA, nickel(II) ethylenediaminediacetate; NTA[Ni(II)], nickel(II) nitrilotriacetic acid; POPC, 1-palmitoyl-2-oleoyl-*sn*-glycero-3-phosphocholine; DOGS-NTA[Ni(II)], 1,2-dioleoyl-*sn*-glycero-3-{[*N*-(5-amino-1-carboxypentyl)iminodiacetic acid]succinyl}nickel salt; POPG, 1-palmitoyl-2-oleoyl-*sn*-glycero-3-[phospho-*rac*-(1-glycerol)]; R1, spin-labeled side chain; TM, transmembrane segment; TPX, trademark for polymethylpentene; W_{ex}, rate of Heisenberg exchange.

10.1021/bi015828s CCC: $22.00
Published on Web 12/29/2001

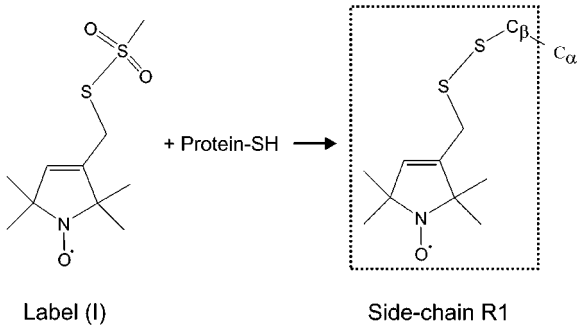

FIGURE 1: Reaction of the methanethiosulfonate reagent **I** with cysteine to generate the side chain designated R1.

the lifetime of a collision complex. The theoretical foundations of HE and some of the many biological applications of HE have been described elsewhere (*12*, *13*).

In the study presented here, we employ HE between R1 residues in a membrane protein and a paramagnetic Ni(II) complex to identify R1 residues that are in the proximity of the membrane−aqueous interface. The experimental strategy is to produce a distribution of Ni(II) localized at the interface using a lipid chelate that binds transition metal ions with high affinity on its headgroup. Lateral diffusion of the lipid Ni(II) chelate is unrestricted, and collisions with the membrane protein will occur. However, only R1 residues that lie on the outer surface of the protein and near the membrane−aqueous interface will have a relatively high level of HE as a result of the collision.

Ni(II) has been selected as the paramagnetic probe because of the short T_{1e} relaxation time of Ni(II) ion and complexes. Under this condition, the interaction between Ni(II) and the nitroxide is dominated by HE with little contribution from through-space dipolar interaction (*14*, *15*). Moreover, HE with fast-relaxing metal ions, like Ni(II), is an effective T_{1e} relaxation pathway for the nitroxide, and the HE rate (W_{ex}) can be determined from the changes produced in the nitroxide T_{1e} (*13*). Changes in the nitroxide T_{1e} can be measured by either power saturation methods (*16*, *17*) or saturation recovery EPR (*18*, *19*).

For this initial study, a commercially available lipid Ni(II) chelate designed for two-dimensional crystallization of membrane proteins was employed (*20*, *21*). The affinity of the lipid chelate (DOGS-NTA) for Ni(II) is similar to that of NTA alone [$K = 10^{8.4}$ at pH 6.7 (*22*)]. As shown in the model of Figure 2, DOGS-NTA contains a spacer between the lipid-anchoring diglyceride moiety and the NTA chelate that extends the metal center a maximum of ≈14 Å above the interface in the extended configuration. Thus, Ni(II) in the aqueous environment will be confined to a slab with a thickness of ≈14 Å at the membrane−aqueous interface.

KcsA, a prokaryotic potassium channel of known structure, has a number of advantageous properties that make it a good choice as a model system for this study. For example, KcsA can be overexpressed at high levels in bacteria, purified to near homogeneity, and functionally reconstituted in a quantitative manner (*23*, *24*). KcsA is a homotetramer surrounding a central 4-fold symmetry axis with each individual subunit contributing two transmembrane α-helices (*25*). The surface-exposed residues on the outer half of the protein shown in Figure 2 were chosen for substitution by R1 and subsequent investigation of the interaction with DOGS-NTA[Ni(II)].

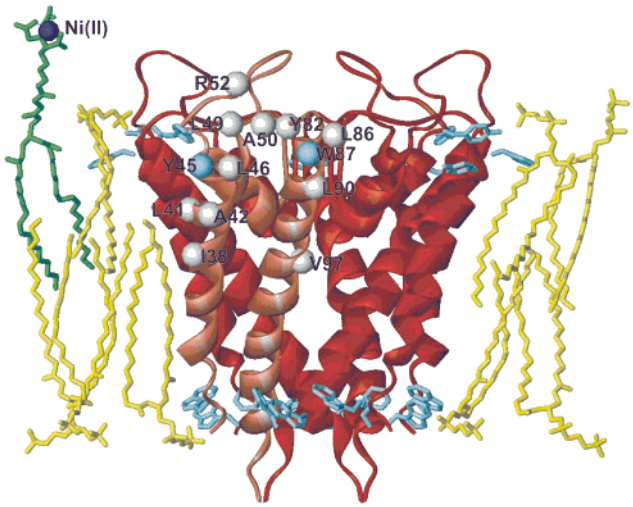

FIGURE 2: Ribbon diagram of KcsA embedded in a membrane consisting of POPC and DOGS-NTA[Ni(II)] lipids. Sites on KcsA where R1 was substituted are identified as spheres on the α-carbons on one of the four identical subunits (shown in light red). Residues I38−R52 are located on TM1, L86−V97 are located on TM2, and Y82 is near the pore. Aromatic residues near the two membrane−aqueous interfaces are shown in blue on all four subunits. POPC is shown in yellow, and DOGS-NTA is shown in green in an extendend conformation with the Ni(II) ion in the chelate shown in dark blue.

The results indicate that, as expected, DOGS-NTA[Ni(II)]−nitroxide interactions are dominated by HE. W_{ex} is greatest at residues that are exposed toward the water−lipid boundary and nearby regions, but falls off rapidly with increasing distance from the interface. In contrast, an R1 residue exposed to the aqueous phase, but located near the symmetry axis of the protein (Y82R1), is unavailable for HE interaction with the Ni(II) chelate.

MATERIALS AND METHODS

Expression of Cysteine Substitution Mutants, Purification, and Spin Labeling. The cysteine substitution mutants and their spin-labeled derivatives are designated by giving the original residue, the amino acid number, and the new residue (R1), in that order. Mutants Y82R1, L86R1, W87R1, L90R1, and V97R1 have been previously described (*26*). The eight remaining mutants were generated by polymerase chain reaction cassette mutagenesis and verified by sequencing the insert on both strands. Mutants were overexpressed, purified, and spin labeled as previously described (*26*). Briefly, *Escherichia coli* (Novablue, Novagen, Madison, WI) membranes containing overexpressed KcsA were solubilized with dodecyl maltoside, and KcsA was purified in two sequential steps, a cation-exchange chromatography column (Resource S, Pharmacia, Piscataway, NJ) followed by a metal chelate affinity column (Ni−NTA Superflow, Qiagen, Chatsworth, CA). Spin labeling was carried out between the two columns. The detergent was exchanged with CHAPS while KcsA was immobilized on the Ni−NTA resin.

Reconstitution and EPR Measurements. KcsA was reconstituted in a 4:1 molar mixture of POPC and DOGS-NTA-[Ni(II)] lipids (Avanti Polar Lipids, Alabaster, AL) by gel filtration on Sephadex G-25 (Pharmacia) following the method of Green and Bell (*27*). The protein:lipid molar ratio was ∼1:1000, and the solution contained 20 mM morpholi-

nopropanesulfonic acid, 140 mM NaCl, 10 mM KCl, and 0.02% NaN_3 (pH 6.7). Vesicles containing spin-labeled KcsA were pelleted by ultracentrifugation and resuspended in the buffer described above. To remove Ni(II) from the lipid headgroups, the sample was diluted 1:3 with the buffer described above containing 50 mM EDTA. The samples were loaded into gas permeable TPX capillaries for EPR measurements under nitrogen flow. First-derivative absorption spectra were measured on an X-band Varian E-109 spectrometer fitted with a loop-gap resonator (*28*). Spectra were recorded at 100 G scan widths under field-frequency lock. The incident microwave power was 2 mW unless otherwise stated.

The collision parameter Π was measured by power saturation of the first-derivative $m_I = 0$ resonance line as previously described (*16*, *29*). Briefly, the peak-to-peak amplitude (A) of the resonance line as a function of microwave power was fit to

$$A = I\sqrt{P}[1 + (2^{1/\epsilon} - 1) \times P/P_{1/2}]^{-\epsilon} \quad (1)$$

where P is the incident microwave power, $P_{1/2}$ is the power at which A is one-half of its unsaturated value, ϵ is a factor related to the homogeneity of the line, and I is a scaling factor (*17*). The fit provides values of ϵ and $P_{1/2}$. Ni(II) was then removed from the lipid headgroups by addition of excess EDTA (see above), followed by five freeze−thaw cycles, and $P_{1/2}$ was determined again. The change in $P_{1/2}$, $\Delta P_{1/2}$, due to the presence of Ni(II) in the lipid headgroups, is proportional to the rate of exchange between the spin-label and Ni(II), W_{ex}, according to

$$\Delta P_{1/2}/\Delta H = [P_{1/2}(\mathrm{Ni}) - P_{1/2}(\mathrm{EDTA})]/\Delta H \propto W_{ex} \quad (2)$$

where $P_{1/2}$(Ni) and $P_{1/2}$(EDTA) are the values in the presence and absence of Ni(II) in the lipid headgroups, respectively, and ΔH is the peak-to-peak line width of the center line. The parameter $\Delta P_{1/2}/\Delta H$ was normalized to the same parameter for 2,2-diphenyl-1-picrylhydrazyl (DPPH), a common reference sample, to account for instrument variability according to

$$\Pi = (\Delta P_{1/2}/\Delta H)/[\Delta P_{1/2}(\mathrm{DPPH})/\Delta H(\mathrm{DPPH})] \propto W_{ex} \quad (3)$$

The line width changes upon addition of EDTA were negligible in all cases, verifying the constancy of T_{2e} of the nitroxide, as required for use of eqs 2 and 3.

RESULTS

Methodology and the Model System. On the basis of the crystal structure of KcsA, 13 lipid- or solvent-exposed residues were identified for this study (Figure 2). Exposed residues show minimal interaction with other parts of the channel and are likely to experience collisions with lipid or solvent molecules. Eight of these residues (I38, L41, A42, Y45, L46, L49, A50, and R52) are located on the first transmembrane helix (TM1) of KcsA, the peripheral or outer helix that traverses the bilayer from the inside to the outside. Four additional residues (L86, W87, L90, and V97) are located on the second transmembrane helix of KcsA, the central or inner helix that traverses the bilayer from the outside to the inside. The last residue (Y82) is located close to the 4-fold symmetry axis of KcsA, shielded from interactions with the bilayer by virtue of its central position. All selected residues are located on the extracellular half of the known KcsA crystal structure. In this part of the channel, the structural model is contiguous and well supported by both crystallographic and spin labeling data (*25*, *26*, *30*).

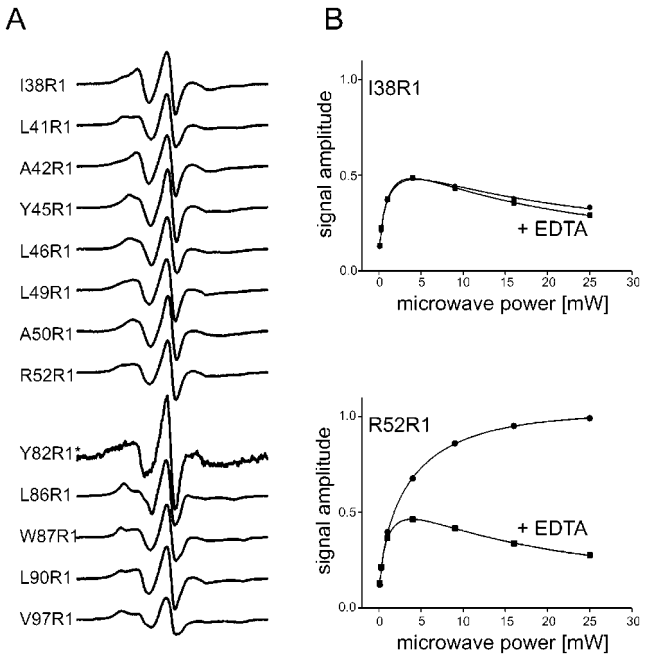

FIGURE 3: EPR spectra and power saturation curves. (A) First-derivative absorption spectra of R1 mutant channels reconstituted in POPC/DOGS-NTA[Ni(II)] liposomes. Spectra were acquired at room temperature over a scan width of 100 G. Spectra are normalized to reflect approximately equal numbers of spin. Y82R1* was labeled using a mixture of reagent **I** (Figure 1) and a diamagnetic analogue (*26*). (B) Power saturation of two spectra [I38R1 (top) and R52R1 (bottom)]. The amplitude of the central resonance line ($m_I = 0$) is plotted as a function of incident microwave power. The solid line is a fit to eq 1 (see Materials and Methods). EDTA was added to displace Ni(II) from the lipid headgroups (see the text): (●) in the presence of Ni(II) in the headgroups and (■) after addition of EDTA.

Each selected residue was mutated individually to a cysteine and subsequently derivatized with a thiol-specific nitroxide reagent to yield the side chain R1 (Figure 1). The purified and labeled channel mutants were next reconstituted into phospholipid vesicles consisting of POPC and 20 mol % DOGS-NTA[Ni(II)]. The equilibrium free concentration of Ni(II) should not exceed 15 μM under the experimental conditions employed here. Such low levels of free Ni(II) have no measurable effect on nitroxide relaxation under these conditions. In combination with site-directed spin labeling, it is thus possible to strictly control the distribution of two paramagnetic species on or near a functionally reconstituted membrane protein. Via movement of the nitroxide along the surface of the protein, the effect of Ni(II) on nitroxide relaxation can be determined in a position-dependent manner.

EPR Spectra and Saturation Behavior. The first-derivative EPR spectra of the labeled and reconstituted KcsA mutant channels studied here have been previously published (*26*, *30*), and are reproduced in Figure 3A for reference. The spectra of all R1 residues on the first transmembrane helix (between positions 38 and 52) indicate relatively high side chain mobility, consistent with their location on solvent-

exposed helical sites (*31*, *32*). The spectra of R1 residues located on the second transmembrane helix (between positions 86 and 97) are more complex and in general indicate a lower overall mobility compared with TM1 residues. We have previously attributed this lower mobility to either local steric interactions of the nitroxide with other parts of the channel or, alternatively, a high degree of internal or backbone rigidity of the second transmembrane segment itself (*26*). Residue Y82R1 is located very close to the symmetry axis of the molecule, and as a result, its spectrum shows evidence of strong spin−spin interaction between nitroxides in adjacent subunits. To reduce the effect of this interaction, residue Y82C was labeled with, on average, less than one spin label per channel, as previously described (*26*). The resulting spectrum of Y82R1* indicates relatively high mobility, and the residue has relatively high rates of collision with the chelate NiEDDA in solution (data not shown).

The presence of 20 mol % DOGS-NTA[Ni(II)] in the lipid headgroup region does not significantly alter the line shape of the spectra shown in Figure 3A. This indicates that $W_{ex} < T_{2e}^{-1}$, and under this condition, power saturation methods can be used to determine the accessibility parameter Π, which is directly proportional to W_{ex} (see Materials and Methods). Figure 3B shows power saturation data from two selected residues. In the presence of DOGS-NTA[Ni(II)], residue R52R1, which is located at the extracellular end of TM1, saturates poorly, as indicated by the monotonic increase in signal amplitude with microwave power. Upon removal of Ni(II) from the chelate by addition of EDTA, R52R1 saturates readily (Figure 3B, bottom panel), demonstrating the loss of the relaxation pathway provided by HE. The saturation behavior of R52R1 in POPC/DOGS-NTA lipids in the presence of EDTA is essentially the same as in POPC/POPG lipids (data not shown). This illustrates that under the conditions employed here, the newly formed NiEDTA complex in solution has no significant effect on nitroxide relaxation. In contrast to the case for R52R1, the saturation behavior of residue I38R1, located approximately in the middle of the bilayer on TM1, is unaffected by the removal of Ni(II) from the DOGS-NTA complex (Figure 3B, top panel). This demonstrates the lack of HE between DOGS-NTA[Ni(II)] and R1 at this site.

For each site that was investigated, a value for the accessibility parameter Π was computed from the difference in saturation curves in the presence and absence of Ni(II). Figure 4 summarizes the results in a plot of Π as a function of residue position in the sequence. As is evident, the enhancement is largest for residues exposed at the water−lipid boundary and the immediately adjacent solvent layer (e.g., R52R1), and is effectively absent for residues located approximately in the middle of the bilayer (e.g., I38R1). The Ni(II) relaxation enhancement decays rapidly with increasing immersion depth of R1 in the bilayer on both TM1 (I38R1−R52R1) and TM2 (L86R1−V97R1) (see Figure 2). Residue Y82R1 does not project toward the bilayer, but instead is water-exposed and is located close to the symmetry axis. The Π value for this position is also very low and experimentally indistinguishable from zero.

Figure 5 shows the above results mapped onto the solvent accessible surface of KcsA. The residues can be broadly grouped into two categories, those with a relatively large relaxation enhancement (shown in red, Π > 0.1), and those

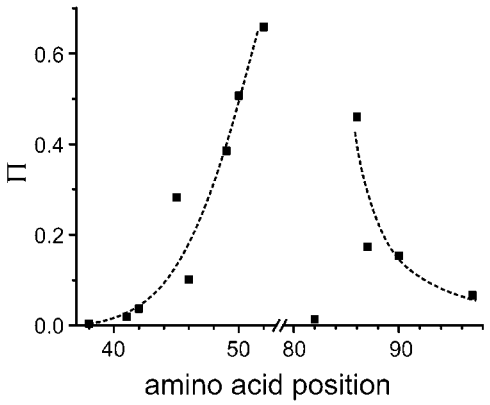

FIGURE 4: Π as a function of residue position. Residues I38−R52 are located on TM1, L86−V97 are located on TM2, and Y82 is near the pore. The dashed lines are shown to guide the eye and are of no theoretical significance.

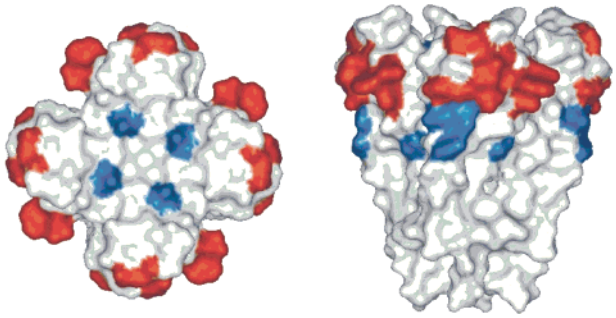

FIGURE 5: Surface rendering of Π data. Top (left) and side (right) views of KcsA. Areas with relatively high rates of collisions (Π > 0.1) are shown in red, and areas with low rates of collisions (Π < 0.1) are shown in blue on all four subunits. Note the low rate of collision for the surface area projected by Y82R1 (central blue area in left panel).

with a low or even no measurable effect on nitroxide relaxation (shown in blue, Π < 0.1). Such a representation shows a ring of highly accessible residues around the circumference of the protein. Among these residues are the two aromatic residues, Y45 and W87. This ring of accessible residues, therefore, coincides with the location of the water−lipid boundary as expected on the basis of the location and projection of aromatic residues in the crystal structure. Residues that are excluded from the water−lipid boundary region, because they either are buried deep in the bilayer or are protected from the membrane−aqueous interface by intervening residues, exhibit low to no detectable effects of Ni(II). The result of residue Y82R1 is particularly important in this respect, because it illustrates that solvent-exposed residues that are not located at the water−lipid boundary can indeed be recognized as such with this method. This was not the case with a paramagnetic reagent in solution.

In two previous EPR studies on KcsA, paramagnetic reagents in solution were used to determine the location of the outer (on TM1) and inner (on TM2) water−lipid boundary (*26*, *30*). The results of the study presented here are in excellent agreement with these previously determined results. A sharp increase in the collision rate for the highly polar NiEDDA complex in solution was observed between L49R1 and R52R1 on TM1 and between W113R1 and R117R1 on TM2, indicating that the transmembrane α-helices are crossing the water−lipid boundary between those residues. On both sides of the membrane, a layer of aromatic

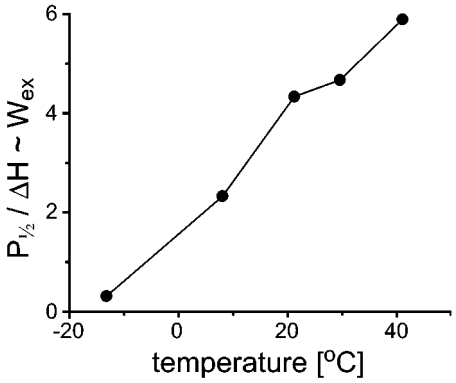

FIGURE 6: Temperature dependence of $P_{1/2}$, normalized to the central line width, for the R52R1 mutant in the presence of DOGS-NTA[Ni(II)].

residues was thus found to lie within the hydrophobic part of the bilayer, but very close to the aqueous phase as judged by the accessibility to the NiEDDA complex.

Mechanism of Relaxation Enhancement. Previous studies have found that the mechanism of nitroxide relaxation enhancement by Ni(II) salts was dominated by HE (*15*), and this has also been found to be the case for NiEDDA complexes in solution (C. Altenbach and W. L. Hubbell, unpublished). As a simple test of the effectiveness of the HE mechanism for R1 relaxation enhancement by DOGS-NTA[Ni(II)] in bilayers, the temperature dependence of $(P_{1/2}/\Delta H) \propto W_{ex}$ was investigated. The R52R1 channel mutant was chosen because the relaxation enhancement is greatest at this position. Because HE requires direct collision between the paramagnetic species, $P_{1/2}/\Delta H$ should increase with increasing temperature due to the increase in the lateral diffusion rate. On the other hand, relaxation enhancement due to dynamic dipolar effects decreases with increasing temperature due to the decrease in the lifetime of the encounter complex (*13*). The data in Figure 6 show an increasing relaxation enhancement with increasing temperature, indicating that HE dominates the enhancement mechanism.

DISCUSSION

Lateral Diffusion Determines the Collision Rate. This study takes advantage of the magnetic interaction between two paramagnetic species, a nitroxide spin-label introduced in a site-specific manner on a membrane protein and a metal ion spin probe localized near the headgroup region of the lipid bilayer. Among transition metal ions with high stability constants for NTA, Ni(II) is an excellent choice. Both Ni(II) salts and complexes have fast spin−lattice relaxation rates, ensuring that magnetic interactions with nitroxides will be dominated by HE (*15*). A HE mechanism of interaction requires orbital overlap during collisions and thus provides high spatial resolution of the metal−nitroxide interaction. The spatial resolution of the technique is limited by the fairly wide distribution of Ni(II) at the interface and not by the magnetic interaction itself (see below). An additional advantage of a spin probe with a fast spin−lattice relaxation rate is that its EPR spectrum is not observed and hence does not interfere with the measurement of the nitroxide EPR spectrum.

The rate of collision between the protein and DOGS-NTA-[Ni(II)] is proportional to the product of the concentration of DOGS-NTA[Ni(II)] and its lateral diffusion constant. The local concentration of Ni(II) at the membrane−aqueous interface is ≈0.3 M, assuming that it is confined to an ∼14 Å slab at the surface and that the area per lipid is 70 Å^2. For this concentration of Ni(II) chelate in solution, W_{ex} with an exposed nitroxide on a protein would be high, leading to pronounced nitroxide line broadening. The relatively low values of W_{ex} observed in the membrane are apparently due to the low diffusion rate of the DOGS-NTA[Ni(II)] complex in the bilayer. A typical lateral diffusion constant for a lipid in a phospholipid bilayer is $\sim 10^{-8}$ cm^2/s (*33*), or ∼3 orders of magnitude smaller than typical values for three-dimensional diffusion of small molecules in water. With this diffusion coefficient, a simple hexagonal lattice model of lipid packing predicts a collision rate of a lipid with a protein of ∼4 MHz (*34*). How does this expected collision rate compare with the experimentally measured exchange rate? The proportionality factor between Π and the exchange rate for the R1 side chain has been determined from pulsed saturation recovery to be ∼2 MHz (C. Altenbach, W. Froncisz, and W. L. Hubbell, unpublished results). Thus, the highest value of Π on KcsA (0.65 for R52R1) corresponds to an exchange rate of ∼1.3 MHz. Because every collision does not necessarily lead to HE, this is on the order of magnitude expected from the above calculation.

Spatial Resolution and Steric Effects. Figure 2 indicates that the vertical distance above the membrane (into the aqueous phase) that is accessible to Ni(II) is ∼14 Å. Although the rather long linker between the diglyceride and NTA moieties limits the spatial resolution of the technique, it does have the advantage that the collision rates are measurable over a finite range of nitroxide positions. If the NTA moiety were strongly constrained by a short linker, collision rates might be so small as to be undetectable except for the rare cases where the position of the R1 side chain with respect to NTA[Ni(II)] is optimal. Nevertheless, it may be possible to improve the vertical spatial resolution of the measurement by using a lipid with a somewhat shorter linker. For any lipid chelate having two hydrocarbon chains, vertical fluctuations of the lipid into the aqueous phase are not expected to limit the spatial resolution. Assuming a sharp water−lipid boundary and ≈0.7 kcal/mol contributed by each CH_2 to the free energy of transfer from the membrane to water (*35*), we can estimate that states with vertical displacements of 3 Å would amount to less than 1% of the equilibrium population.

Figure 5 indicates that the rates of collision of DOGS-NTA[Ni(II)] with R1 on KcsA are finite even for sites within the lipid bilayer. Ni(II) complexes are fairly soluble in the bilayer, and even Ni(II) salts partition to a measurable extent into the bilayer interior (*15*). The DOGS-NTA[Ni(II)] complex is probably uncharged at neutral pH (*22*), facilitating the partitioning of the NTA[Ni(II)] moiety into the hydrophobic core of the bilayer. As for NiEDDA (*14*), the rate of collision of DOGS-NTA[Ni(II)] with R1 drops off rapidly with increasing immersion depth. Nevertheless, excursions of the NTA[Ni(II)] complex into the hydrophobic core do limit the spatial resolution of the measurement in the direction of the bilayer. This imprecision could be addressed by using a phospholipid as the lipid anchor for the chelate. The presence of a fixed negative charge in the headgroup region would significantly dampen vertical fluctuations of

the lipid and reduce excursions of the chelate into the interior of the bilayer, thus improving the spatial resolution of the technique.

Local steric effects can be expected to greatly influence the exchange rate in ways that may be difficult to predict. However, by restricting the analysis to those residues that show a high degree of side chain mobility (Figure 3A) and hence high levels of solvent exposure, we can minimize uncertainties in the exchange rate due to steric effects.

Application to Membrane Protein Structure. Among nonrandomly distributed residues in membrane proteins, the abundance of aromatic residues at the interface is particularly striking given their overall scarcity (*36*). This distribution makes them ideal targets for an experimental strategy aimed at identifying interfacial residues. In KcsA, for example, six of the 13 aromatic residues per subunit are exposed toward the interface. Of the three aromatic residues probed in this study, Y45R1 and W87R1 are in the interface (Π values of 0.28 and 0.17, respectively) and Y82R1 is not ($\Pi \approx 0$). Systematic probing of all aromatic residues in a membrane protein of unknown structure could prove to be an efficient way of identifying interface-exposed residues, which would have to lie on two parallel rings separated by a distance equivalent to approximately the thickness of the hydrophobic part of the bilayer (Figure 2). Identification of just a few such residues may sharply limit the number of available folds of a membrane protein.

In proteins of known structure, an R1 residue introduced at the interfacial boundary may serve as a sensitive means of detecting structural changes during function. Given that the rate of collision of the nitroxide with DOGS-NTA[Ni(II)] is highly sensitive to local steric factors and/or changes in lipid immersion, a subtle local rearrangement may significantly alter the collision rate for a given site on the protein. For instance, it has been proposed that residues on the second transmembrane segment of KcsA must move during gating of the ion channel (*25*, *30*). A nitroxide probe at the intracellular interface may be able to report that movement in a very sensitive manner should it be possible to force the channel population collectively from a closed to an open conformation.

ACKNOWLEDGMENT

We thank Susannah Marshall for technical assistance and Linda Columbus, Carole LaBonne, and Peter Qin for helpful comments on the manuscript.

REFERENCES

1. Wallin, E., and von Heijne, G. (1998) *Protein Sci. 7*, 1029−1038.
2. Arkin, I. T., and Brunger, A. T. (1998) *Biochim. Biophys. Acta 1429*, 113−128.
3. Ulmschneider, M. B., and Sansom, M. S. (2001) *Biochim. Biophys. Acta 1512*, 1−14.
4. Hubbell, W., and Altenbach, C. (1994) *Curr. Opin. Struct. Biol. 4*, 566−573.
5. Hubbell, W. L., Mchaourab, H. S., Altenbach, C., and Lietzow, M. A. (1996) *Structure 4*, 779−783.
6. Hubbell, W. L., Gross, A., Langen, R., and Lietzow, M. A. (1998) *Curr. Opin. Struct. Biol. 8*, 649−656.
7. Feix, J. B., and Klug, C. S. (1998) in *Biological Magnetic Resonance* (Berliner, L. J., Ed.) pp 251−281, Plenum Press, New York.
8. Hubbell, W. L., Cafiso, D. S., and Altenbach, C. (2000) *Nat. Struct. Biol. 7*, 735−739.
9. Leigh, J. S. (1970) *J. Chem. Phys. 52*, 2608−2612.
10. Kokorin, A. I., Zamaraev, K. I., Grigoryan, G. L., Ivanov, V. P., and Rozantzev, E. G. (1972) *Biofizika 17*, 34−41.
11. Berliner, L. J., Eaton, S. S., and Eaton, G. R. (2000) in *Biological Magnetic Resonance*, pp 614, Kluwer Academic/Plenum Publishers, New York.
12. Hyde, J. S., Swartz, H. M., and Antholine, W. E. (1979) in *Spin labeling II. Theory and applications* (Berliner, L. J., Ed.) pp 71−113, Academic Press, New York.
13. Molin, Y. N., Salikhov, K. M., and Zamaraev, K. I. (1980) *Spin exchange: principles and applications in chemistry and biology*, Spinger Verlag, Berlin.
14. Altenbach, C., Greenhalgh, D. A., Khorana, H. G., and Hubbell, W. L. (1994) *Proc. Natl. Acad. Sci. U.S.A. 91*, 1667−1671.
15. Livshits, V. A., Dzikovski, B. G., and Marsh, D. (2001) *J. Magn. Reson. 148*, 221−237.
16. Altenbach, C., Flitsch, S. L., Khorana, H. G., and Hubbell, W. L. (1989) *Biochemistry 28*, 7806−7812.
17. Oh, K. J., Altenbach, C., Collier, R. J., and Hubbell, W. L. (2000) *Methods Mol. Biol. 145*, 147−169.
18. Hyde, J. S. (1979) in *Time Domain Electron Spin Resonance* (Schwartz, R. N., Ed.) pp 1−30, John Wiley and Sons, New York.
19. Altenbach, C., Froncisz, W., Hyde, J. S., and Hubbell, W. L. (1989) *Biophys. J. 56*, 1183−1191.
20. Kubalek, E. W., Le Grice, S. F., and Brown, P. O. (1994) *J. Struct. Biol. 113*, 117−123.
21. Schmitt, L., Dietrich, C., and Tampe, R. (1994) *J. Am. Chem. Soc. 116*, 8485−8491.
22. Dawson, R. M. C., Elliott, D. C., Elliott, W. H., and Jones, K. M. (1986) *Data for biochemical research*, 3rd ed., Oxford Science Publications, New York.
23. Schrempf, H., Schmidt, O., Kummerlen, R., Hinnah, S., Muller, D., Betzler, M., Steinkamp, T., and Wagner, R. (1995) *EMBO J. 14*, 5170−5178.
24. Heginbotham, L., Kolmakova-Partensky, L., and Miller, C. (1998) *J. Gen. Physiol. 111*, 741−749.
25. Doyle, D. A., Cabral, J. M., Pfuetzner, R. A., Kuo, A., Gulbis, J. M., Cohen, S. L., Chait, B. T., and MacKinnon, R. (1998) *Science 280*, 69−77.
26. Gross, A., Columbus, L., Hideg, K., Altenbach, C., and Hubbell, W. L. (1999) *Biochemistry 38*, 10324−10335.
27. Green, P. R., and Bell, R. M. (1984) *J. Biol. Chem. 259*, 14688−14694.
28. Hubbell, W. L., Froncisz, W., and Hyde, J. S. (1987) *Rev. Sci. Instrum. 58*, 1879−1886.
29. Farahbakhsh, Z. T., Altenbach, C., and Hubbell, W. L. (1992) *Photochem. Photobiol. 56*, 1019−1033.
30. Perozo, E., Cortes, D. M., and Cuello, L. G. (1998) *Nat. Struct. Biol. 5*, 459−469.
31. Mchaourab, H. S., Lietzow, M. A., Hideg, K., and Hubbell, W. L. (1996) *Biochemistry 35*, 7692−7704.
32. Columbus, L., Kalai, T., Jeko, J., Hideg, K., and Hubbell, W. L. (2001) *Biochemistry 40*, 3828−3846.
33. Trauble, H., and Sackmann, E. (1972) *J. Am. Chem. Soc. 94*, 4499−4510.
34. Devaux, P., and McConnell, H. M. (1972) *J. Am. Chem. Soc. 94*, 4475−4481.
35. Tanford, C. (1980) *The hydrophobic effect: formation of micelles and biological membranes*, 2nd ed., John Wiley and Sons, New York.
36. Yau, W. M., Wimley, W. C., Gawrisch, K., and White, S. H. (1998) *Biochemistry 37*, 14713−14718.

BI015828S